Available online at www.sciencedirect.com

Manufacturing Letters

Manufacturing Letters 33 (2022) 452–460

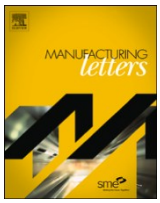

50th SME North American Manufacturing Research Conference (NAMRC 50, 2022)

Modulation-assisted machining of compacted graphite iron with coated carbide tool in dry condition

Juan Sandoval, Aaqib Ali, Patrick Kwon, Yang Guo*

Department of Mechanical Engineering, Michigan State University, East Lansing, 48824, MI, USA

* Corresponding author. Tel.: +1-517-432-3164; *E-mail address:* yguo@msu.edu

Abstract

Compacted graphite iron (CGI) is a new material replacing conventional gray cast iron (FGI) for diesel engine block applications due to its superior mechanical properties. However, widespread adoption of CGI is hindered by its poor machinability, which is reflected by the rapid tool wear especially at higher cutting speeds. In current industrial practice, CGI is usually machined with coated carbide tools at low to medium speeds (< 200 m/min). This study investigates the effect of modulation-assisted machining (MAM) on tool wear in dry turning of CGI with coated carbide tool. A new MAM turning setup is implemented for conducting the longitudinal turning experiments. Tool wear, cutting forces and tool temperature are characterized for both conventional machining (CM) turning and MAM turning at three cutting speeds: 150, 250 and 350 m/min. The results show wear reduction by MAM is not significant at the low cutting speed (150 m/min), but it is quite significant at the higher cutting speeds (250 and 350 m/min). The cutting force and temperature results can be well correlated with the wear results, revealing the dependency of the forces and temperature on the tool wear and the severity of iron adhesion. This study demonstrates the potential of MAM in enhancing the productivity of machining CGI with the coated carbide tool. The results are also useful for better understanding the wear mechanism in cutting CGI with the coated carbide tool.

Keywords: tool wear; tool temperature; difficult-to-cut material; vibration-assisted cutting; adhesion;

1. Introduction

Compact graphite iron (CGI) has emerged as a promising candidate material to replace gray cast iron for making diesel engine blocks and heads [1]. Unlike the flake-shaped graphite in gray cast iron (or flake graphite iron (FGI)), CGI has vermicular-shaped graphite which integrates better mechanically with the iron matrix. As a result, CGI provides 2 to 5 times better strength-to-weight and stiffness-to-weight ratio compared to more common FGI [2]. Engine blocks and heads made of CGI can be lighter and withstand higher combustion pressure, leading to increased fuel economy and reduced emissions. However, CGI has very poor machinability which is a major barrier for wider adoption [3]. For comparison, gray cast iron can be machined using cubic boron nitride (CBN) tools at high cutting speeds up to 800 m/min. However, CBN tooling cannot be used with CGI due to the rapid chemical wear [4]. Instead, CGI is often machined with coated carbide tools at cutting speeds typically below 200 m/min. This leads to significantly lower production rates and higher costs for CGI components compared to FGI components [5,6].

The challenge for machining CGI is even greater in continuous cutting operations such as turning, boring and drilling [4,7]. Compared to intermittent cutting operations such as milling, the continuous cutting creates more intense heating on the tool and prevents cutting fluids from accessing the intimate tool-chip interface [8,9]. These conditions further accelerate the rapid tool wear in machining CGI. One strategy to address this challenge is to develop better tool materials or coatings which can withstand the severe mechanical and thermal load and resist the thermally activated reactions between the tool and work material during cutting. So far, no

commercially available cutting tool has been able to significantly improve the productivity of machining CGI [10–12]. The progress in developing new tool coatings in this regard is also limited [13,14]. Another strategy for addressing this challenge is to develop better machining processes which can mitigate the severe tool contact condition during cutting such that the rapid tool wear is not activated for the commonly used cutting tools. Following this strategy, a novel machining process, i.e., modulation-assisted machining (MAM) [15] has shown promising prospect for addressing the difficulty of cutting CGI [16]. It has been demonstrated that MAM can greatly suppress the rapid chemical wear of CBN tools in cutting CGI at high speeds (> 500 m/min) [16,17]. The reduction in tool wear with CBN tools is so significant that it makes it possible to seriously consider CBN tools in machining CGI. The benefit of MAM for machining CGI should not be limited to the CBN tools. It is of great interest to also investigate the effect of MAM on the wear performance of coated carbide tools in machining CGI.

Compared to CBN tools, coated carbide tools are more widely available and used in more machining applications owing to the significantly lower tool cost. Indeed, current industrial practice in machining CGI is primarily using the coated carbide tools. However, the applicable cutting speed is often limited to below 200 m/min and flood coolant must be applied due to the poor machinability of CGI [18]. If the cutting speed for the coated carbide tools can be significantly increased and the coolant usage can be reduced, the machining cost for CGI component will be greatly saved. With such motivations, this study will investigate MAM turning of CGI with coated carbide tool in dry condition. A new MAM turning device is developed to conduct longitudinal turning experiments. The progression of tool wear together with the cutting force and temperature is measured and characterized for a range of cutting speeds (150, 250 and 350 m/min) for both conventional and MAM turning. The results show MAM can substantially reduce tool wear and enable dry machining of CGI with coated carbide tool at much higher speeds than conventional turning. The correlations of tool wear with cutting force and tool temperature are also discussed. The potential of MAM in improving the machinability of other difficult-to-cut materials can be also inferred from this study.

2. Modulation-Assisted Turning

Modulation-assisted machining is a novel machining process in which a controlled low-frequency (< 500 Hz) tool vibration is superimposed onto the tool feed motion during cutting, such that a continuous cutting process, e.g., turning, boring, and drilling, can be divided into a series of discrete cutting events [15,19]. The benefits of MAM include better chip management [20], improved cutting fluid penetration [21], and reduced chip deformation [22]. Figure 1 illustrates the MAM turning process. In conventional machining (CM) turning (Fig. 1a), the constant feedrate generates a parallel helical tool path on the revolving workpiece surface. The tool path does not intercept between successive revolutions, so the tool is always engaged with the workpiece leading to continuous cutting. The uncut chip thickness is also a constant. In contrast, when a properly controlled tool vibration is applied in the tool feed direction (Fig. 1b), the resultant feedrate becomes modulated which generates a sinusoidal wave tool path on the revolving workpiece surface. When the wave tool path is out of phase between successive revolutions and the wave amplitude is high enough, the tool path then intercepts between successive revolutions. This means the tool is periodically disengaged from the cut leading to a discrete cutting process. The wave tool path shown in Fig. 1b has the phase of $\varphi = \pi$. The vibration frequency and amplitude required to achieve tool path interception or discrete cutting at $\varphi = \pi$ are [15],

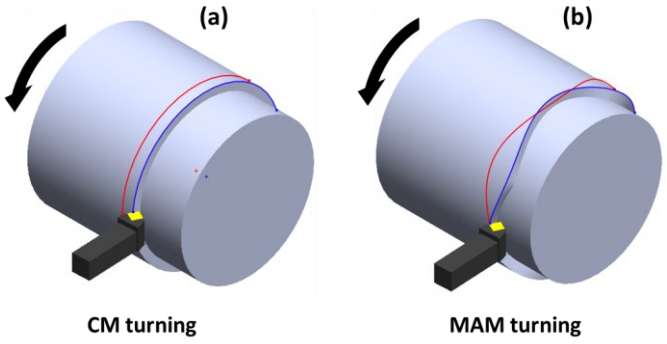

Fig. 1. Schematic of (a) CM and (b) MAM turning

$$\frac{f_m}{f_w} = \frac{2N+1}{2}, N = 0,1,2,... \quad (1)$$

$$A \geq \frac{h_0}{2} \quad (2)$$

where f_m is the vibration frequency; f_w is the workpiece rotation frequency (=RPM/60); A is the vibration amplitude; and h_0 is the tool feed per revolution. Equation (1) is the condition for generating wave tool path of phase $\varphi = \pi$. It states that the ratio of vibration frequency to rotation frequency should be equal to half integer values, i.e., 0.5, 1.5, 2.5, 3.5, etc. Equation (2) states that the amplitude threshold for discrete cutting is the half of the feed per revolution (or peak-to-peak amplitude ($2A$) threshold is the feed per revolution). The amplitude threshold corresponding to $\varphi = \pi$ is the smallest amplitude threshold. Other φ values will lead to higher amplitude thresholds for achieving discrete cutting. At the extreme, discrete cutting is not possible at phase $\varphi = 0$ or 2π (in phase) because the wave tool path becomes always parallel between successive revolutions.

3. Materials and Methods

Figure 2 shows the MAM turning setup developed for this study. The setup is implemented on a Haas TL-1 toolroom lathe. The tool vibration device consists of a stationary frame, two linear guides, a moving stage, and a piezo stack actuator. The turning tool holder is fixed to the moving stage which is supported by the linear guides whose rails are fixed on the

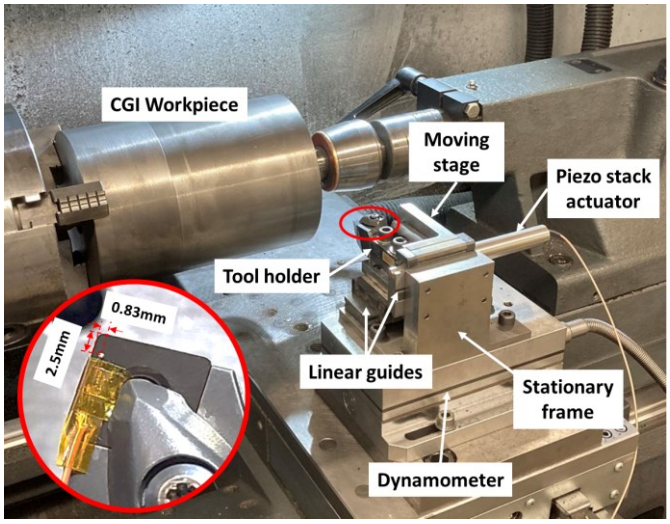

Fig. 2. Experimental setup for MAM turning

stationary frame. The linear guides allow only linear motion but restrict bending and rotation of the moving stage. The casing of the piezo stack actuator is fixed to the stationary frame while its actuator head is connected to the moving stage. The vibration of the turning tool is driven by the piezo stack actuator. The piezo stack actuator used in this study has a stroke of 0.1 mm and can generate a maximum driving force of 4000 N. During MAM turning, the traditional turning parameters including workpiece rotation speed (RPM), tool feed per revolution, and depth of cut are controlled by the lathe; the frequency and amplitude of the turning tool vibration are controlled by the sinusoidal driving voltage applied to the piezo stack actuator. The driving voltage is produced by a waveform generator (BK 4007B) and a power amplifier (MMech PX200).

To enable cutting force measurement, the tool vibration device is mounted onto a Kistler dynamometer plate (9257B) which is fixed onto the carriage of the lathe. The force signal is recorded using a data acquisition system with a sampling rate of 5000/s and processed with a low-pass filter with a cutoff frequency at 500 Hz. Furthermore, tool temperature is measured using a 36 AWG K-type thermocouple secured on the tool rake face with a polyimide film tape (see inset of Fig. 2). The thermocouple junction is positioned at the location that is 0.83 mm from the side (main) cutting edge and 2.5 mm from the end (minor) cutting edge. This location is chosen based on our trials: it is the location at which the thermocouple junction will not be disturbed by the chip flow but is as close to the tool-chip interface as possible to estimate the tool temperature. The temperature history is recorded at a sampling rate of 1/s using a digital thermometer (Fluke 54-II). Note the measured temperature is not exactly at the tool-chip interface, but it should be sufficient to use as a reference of tool temperature for comparison among different cutting conditions.

The CGI workpieces (from SinterCast AB) have hollow cylindrical shape with an outer diameter of 145 mm and an inner diameter of 98 mm, and a length of 204 mm. The grade is classified as GJV-450 by the standard ISO 16112:2017 with a tensile strength of 450 MPa. The microstructure contains graphite agglomerations of vermicular shape, and the matrix is fully pearlitic. The coated carbide insert used for turning is Sandvik Coromant SNMA 12 04 08-KR 3205, which has two-layer TiCN and Al_2O_3 coating on the rake face and three-layer TiCN, Al_2O_3 and TiN coating on the flank face [23]. The used toolholder is DSBNR 2020K which results in -6° rake angle and 15° side cutting edge angle.

Table 1 lists all the turning tests in this study. All tests are conducted in dry condition. The feedrate (h_0 = 0.04 mm/rev) and the depth of cut (d = 1.5 mm) are not varied while the cutting speed (V_c) is varied at three levels, i.e., 150, 250 and 350 m/min, for both CM and MAM turning. For MAM turning, the frequency ratio (f_m/f_w) is controlled to have a half integer value according to Eq. (1), so the phase of the wave tool path is always at $\varphi = \pi$. The frequency ratio is 9.5 for V_c = 150 and 250 m/min and is 6.5 for V_c = 350 m/min. With the two different frequency ratios, the vibration frequency for V_c = 250 and 350 m/min are roughly the same (both in the range ~90 – 110 Hz). The frequency varies within a range in each MAM turning test which is to accommodate the change of f_w at different workpiece diameter. The vibration amplitude is controlled by the sinusoidal driving voltage amplitude. The peak-to-peak amplitude of the driving voltage is set to V_{pp} = 150 V for all MAM turning tests. This driving voltage is corresponding to a peak-to-peak tool vibration amplitude ($2A$) of about 90 µm calibrated at the no-cutting condition.

Table 1. Turning test conditions

Test name	Cutting Speed (m/min)	Feedrate (mm/rev)	Depth of cut (mm)	f_m/f_w	f_m (Hz)	V_{pp} (V)
CM-150	150	0.04	1.5	-	-	-
CM-250	250	0.04	1.5	-	-	-
CM-350	350	0.04	1.5	-	-	-
MAM-150	150	0.04	1.5	9.5	54-67	150
MAM-250	250	0.04	1.5	9.5	90-112	150
MAM-350	350	0.04	1.5	6.5	86-108	150

For each turning test, the cutting is temporarily stopped at every 1.2 km cutting distance for tool wear characterization. At the end of each interval, the tool is first cleaned with ethanol in an ultrasonic cleaner, and then tool wear is observed and measured using a Nikon Eclipse LV100ND microscope and Keyence VHX6000 digital microscope. After the measurement, the turning test is resumed with the same tool for the next interval. The turning test will no longer resume (fully stopped) if the measured flank wear reaches more than 300 µm or the total cutting distance reaches 7.2 km. The latter criterion is implemented to save the workpiece material. At the final stop of each turning test, the tool is further characterized using an Olympus FluoView 1000 confocal laser scanning microscope (CLSM) to obtain the 3D profile of the wear land of the tool [24]. The tool is also characterized using a JEOL 6610LV scanning electron microscope (SEM) together with energy dispersive spectroscopy (EDS) to identify the exposed or deposited materials on the wear land of the tool. These characterizations are performed both before and after removing the iron adhesion on the tool by etching with HCL (19%) for 45 minutes.

4. Results and Discussion

Figure 3 shows the progression of the flank wear (VB_{max}) with the cutting distance for all the tests. To facilitate comparison, the solid line indicates CM turning while the dashed line indicates MAM turning. The line color is used to distinguish the cutting speed. It clearly shows that MAM turning results in significantly lower wear compared to CM turning results. At V_c = 150 m/min (blue), both CM and MAM turning result in the desired steady state slow wear progression to the cutting distance of 7.2 km. The final VB_{max} is 235 µm and 178 µm for CM and MAM turning, respectively. For CM turning at V_c = 250 m/min (green solid line), the slow wear progression is transitioned to rapid wear progression roughly after cutting 2.4 km. VB_{max} exceeds the flank wear threshold of 300 µm after cutting 3.2 km. At V_c = 350 m/min (red solid line), the rapid flank wear occurs even earlier, resulting in a very steep wear curve. VB_{max} exceeds 300 µm after only cutting about 2 km. In contrast, the rapid flank wear progression is not activated in MAM turning at V_c = 250 and 350 m/min. The two corresponding wear curves (green and red dashed lines) show the steady state slow wear progression all the way to the cutting distance of 7.2 km. The final VB_{max} is 223 and 245 µm for V_c = 250 and 350 m/min, respectively. Although the flank wear increases with cutting speed in both CM and MAM turning, the speed effect on wear is far less significant in MAM turning.

Figure 4 shows the selected Keyence microscope images of the tool edge after turning at V_c = 150 m/min. The coating materials in the worn area can be recognized based on the color: TiN appears gold, Al_2O_3 appears brown and TiCN appears black, which have been confirmed by EDS analysis. In both CM and MAM turning after 1.2 km cutting, a uniform wear land is observed along the cutting edge on both the flank and rake faces. The worn surface on the rake face is larger in MAM than in CM turning. This is because the uncut chip thickness is up to 2 times larger in MAM (see Fig. 1b) resulting in larger tool chip contact on the rake face. However, the flank wear land is clearly smaller in MAM. As cutting distance increases to 7.2 km, the flank wear land grows uniformly along the cutting edge in CM turning but nonuniformly in MAM turning. In MAM, the flank wear land grows mainly on the tool nose and near the

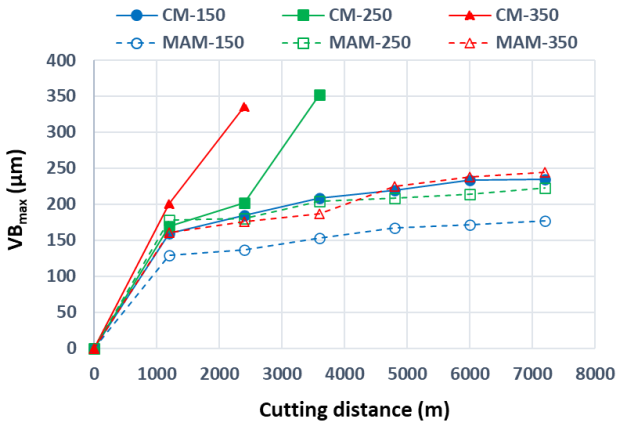

Fig. 3. Progression of flank wear (VB_{max}) with the cutting length for all turning tests

end of the side cutting edge. From the etched tool image, it is found the coating has been breached on the upper portion of the flank wear land in these regions. The material covering the breached area on the unetched tool is identified as iron. In contrast, the breach of tool coating is not observed in CM turning. However, the cutting edge remains very sharp in MAM turning while it appears to be dull in CM turning.

Figure 5 shows the selected Images of the tool edge after turning at V_c = 250 m/min. In CM turning, the wear has not breached tool coating at the cutting distance of 2.4 km based on the fact that no iron adhesion is observed on the tool. However, when reaching the cutting distance of 3.6 km, substantial iron adhesion is observed in a large area of the main flank wear land. The etched tool image shows the actual tool wear in this area is quite deep into the substrate Tungsten Carbide (WC). At the same cutting distance (3.6 km) with MAM turning, no accumulation of iron on the tool is observed, and tool coating has not been breached. At the cutting distance of 7.2 km, mild iron adhesion can be observed on the flank wear land. The etched tool image shows tool coating is breached on the flank wear land mainly on the tool nose area and near the end of the side cutting edge, which contrasts with the case in CM turning. Furthermore, the side cutting edge in MAM is still

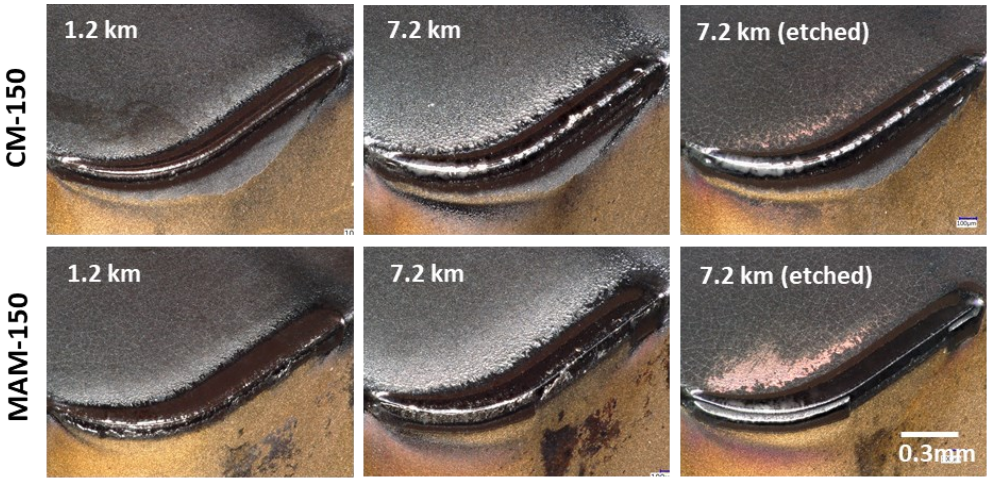

Fig. 4. Keyence digital microscope images of tool edge after turning at V_c = 150 m/min

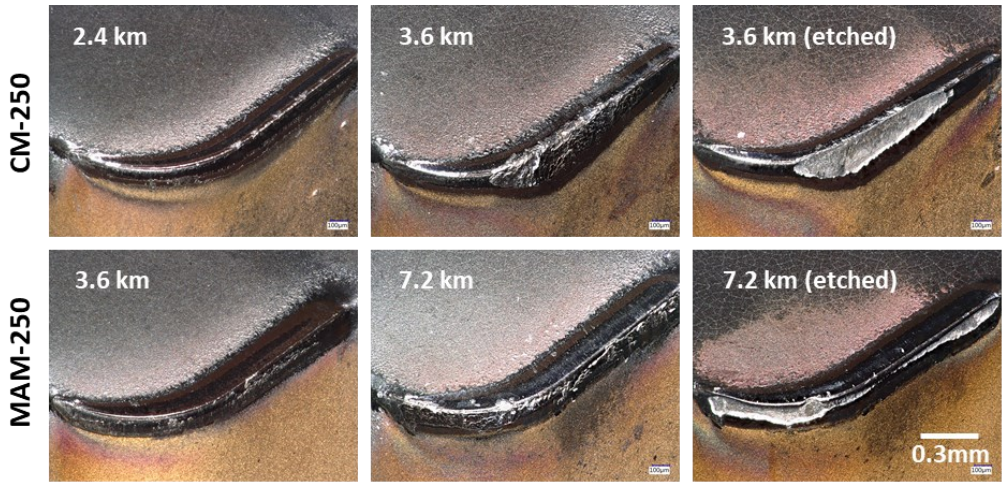

Fig. 5. Keyence digital microscope images of tool edge after turning at V_c = 250 m/min

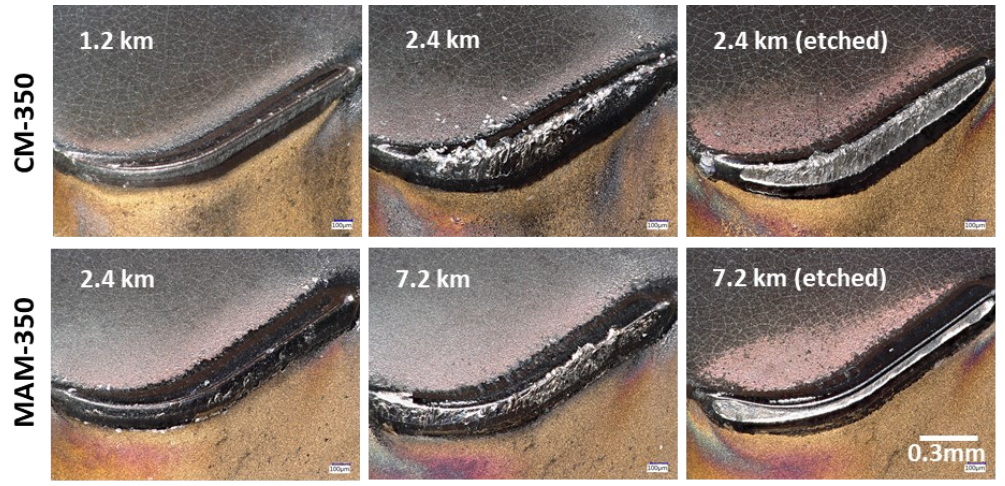

Fig. 6. Keyence digital microscope images of tool edge after turning at V_c = 350 m/min

very sharp after cutting 7.2 km while it is destroyed in CM turning after cutting 3.6 km.

Figure 6 shows the selected images of the tool edge after turning at V_c = 350 m/min. At this speed, substantial iron adhesion is observed after reaching the cutting distance of 2.4 km in CM turning. The iron adhesion spreads along the whole cutting edge on the flank wear land. From the etched tool image, the actual wear beneath the iron adhesion has breached tool coating exposing the WC substrate. In contrast, after reaching the cutting distance of 2.4 km in MAM turning, neither significant iron adhesion nor coating breach is observed on the flank wear land. Significant iron adhesion is observed on the flank after reaching the cutting distance of 7.2 km. The corresponding wear land with the coating breached is more uniformly distributed along the cutting edge. The area of the coating-breached wear land is narrower in MAM turning at the cutting distance of 7.2 km than in CM turning at the cutting distance of 2.4 km. Furthermore, the cutting edge appears much sharper in MAM than in CM turning.

Figure 7 shows the section profiles of the flank wear land of the final etched tools in Figs. 5 and 6. The profiles are measured by CLSM. At each section plane, three profiles are superimposed for comparison, including the new tool profile

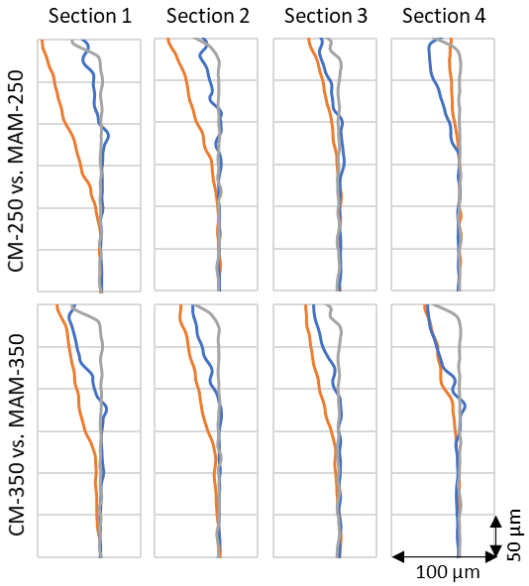

Fig. 7. Section profiles of the main flank wear land of the final etched tool in CM and MAM turning at V_c = 250 and 350 m/min. Gray profile is for new tool, blue for MAM, and orange for CM. The four section planes from left to right are located at 0.66, 0.94, 1.22 and 1.5 mm from the minor cutting edge.

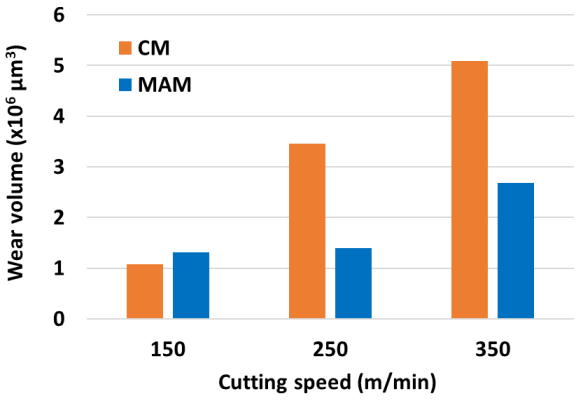

Fig. 8. Wear volume for the main flank wear land of the etched tool in Fig. 4 – 6

(gray), MAM profile (blue) and CM profile (orange). The four section planes (section 1, 2, 3 and 4) are normal to the side cutting edge and located at 0.66, 0.94, 1.22 and 1.5 mm, respectively, from the minor cutting edge. It is evident that the flank wear land resulting from MAM turning is significantly smaller not only in width (vertical direction) but also in depth (horizontal direction). This indicates that the wear reduction by MAM is more significant should the wear volume be compared. Figure 8 shows the calculated wear volume on the flank wear land based on the 3D profile measurements by CLSM. At V_c = 150 m/min, the wear volume is generally low in both CM and MAM turning, despite the slightly higher value in MAM turning. At higher speeds, the wear volume increases substantially in CM turning but moderately in MAM turning. Therefore, the wear volume is significantly lower in MAM than in CM turning at the higher speeds. It should be noted that the tools in MAM after cutting 7.2 km are compared to the tools in CM turning after cutting a much short distance (3.6 or 2.4 km) at the higher speeds. Therefore, the wear reduction in MAM is quite remarkable at higher cutting speeds.

Figure 9 shows the cutting force history for the first three cutting intervals of the turning tests at the higher speeds. Note each cutting interval has the cutting length of 1.2 km. Note also, the forces which appear as force bands in these plots are always oscillating due to the applied tool vibration in MAM turning. The observed force changes in these plots reflect the tool wear effects on cutting forces. For example, the force changes are observed in the initial period of the 1st cutting interval for all turning tests. This should be due to the initial wear development on a new tool while establishing the stable contact between tool and workpiece. In CM turning, the initial tool wear leads to the initial increase and the subsequent decrease in forces while in MAM turning the initial tool wear leads to the continuous increase in forces. These changes are more evident on the feed force (blue) than the primary cutting force (red). In the 3rd interval of CM turning at V_c = 250 m/min and the 2nd interval of CM turning at V_c = 350 m/min, the significant increase in forces, in particular the feed force, can be observed. This can be attributed to the rapid tool wear progression and severe tool adhesion occurring during those intervals (see Figs. 3, 5 and 6). The other cutting intervals show approximately the constant or the steady state forces which correspond to the mild steady state wear progression in those cutting intervals.

To further compare the cutting forces in all the tests, the primary cutting force and the feed force are both averaged over each cutting interval (i.e., over 1.2 km cutting length). Figure 10 plots the averaged forces versus the cutting interval for all the tests. Note the resemblance of these force curves to the wear curves in Fig. 3. These force curves again reflect the influence of tool wear on the cutting forces. It is evident that the tool wear

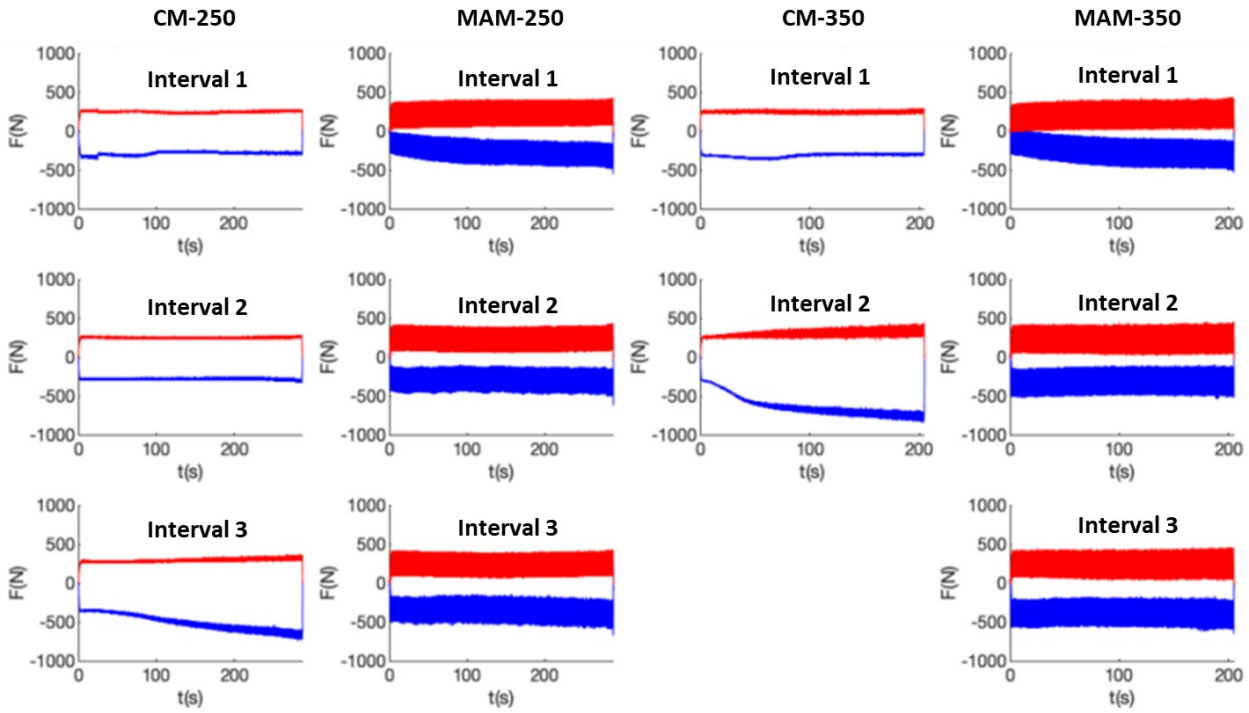

Fig. 9. Primary cutting force (red) and feed force (blue) histories for the first three cutting intervals of the turning tests at V_c = 250 and 350 m/min

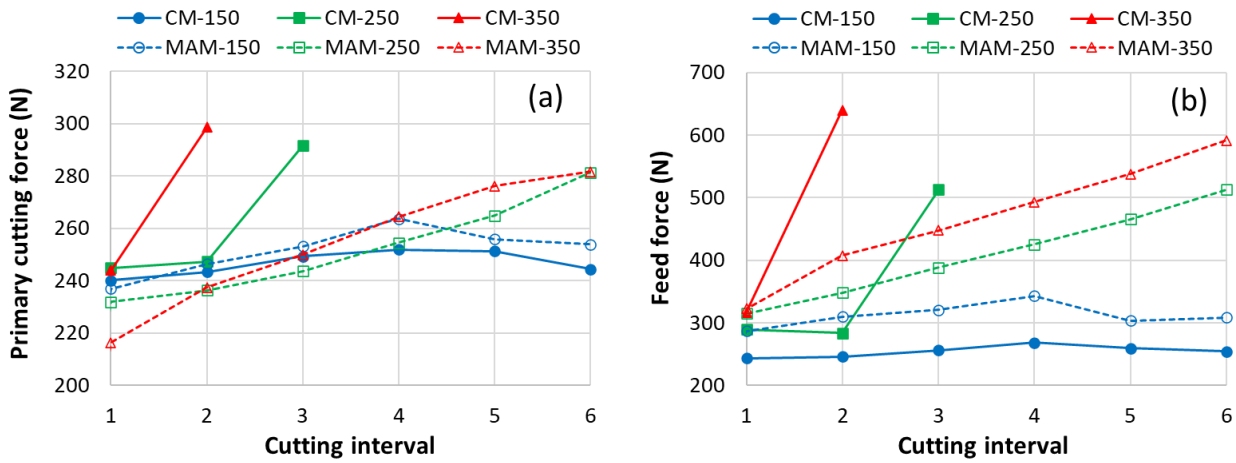

Fig. 10. Averaged primary cutting force and feed force over each cutting interval

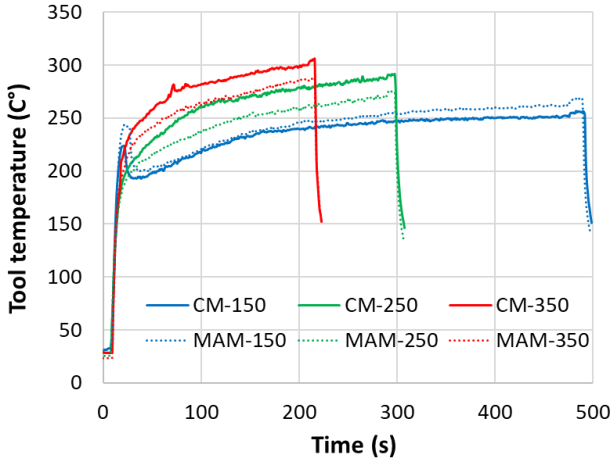

Fig. 11. The tool temperature history during the 1st cutting interval of each test. See measurement setup in Fig. 2.

has a much greater influence on the feed force than the primary cutting force because the major wear is the flank wear. The total area of the flank wear land is equivalent to the tool-work contact area and thus it directly affects the feed force. Besides, the amount of adhesion should also play an important role in affecting the forces. For example, the flank wear land area appears to be roughly the same for CM-150, MAM-250, and MAM-350 (see Figs. 4 – 6), but the respective feed force shown in Fig. 10 is quite different because the severity of tool adhesion in each case is quite different. No adhesion is observed at the cutting distance of 7.2 km in CM-150 (Fig. 4) while adhesion is clearly observed at this cutting distance in both MAM-250 (Fig. 5) and MAM-350 (Fig. 6). It is also evident the adhesion is more severe in MAM-350 than in MAM-250 based on both unetched and etched tool images. Note the coating breached area after etching is equivalent to the adhesion covered area before etching. From these observations, the ranking of the feed force matches the ranking of the severity of adhesion in the three tests.

Figure 11 shows the tool temperature history in the first cutting interval of each turning case. Note the tool temperature is measured at a fixed location on the rake face that is 0.83 mm from the side cutting edge and 2.5 mm from the end cutting edge (see the inset of Fig. 2). In all cases, the tool temperature increases very rapidly during the first few seconds after the cutting starts. The rate at which the temperature increase gradually decreases; the rate appears to approach a nearly constant value at which the temperature increases slowly and steadily. Since the cutting length of each interval is the same, the higher cutting speed results in the shorter temperature history curve. By comparing these curves, it is evident the tool temperature increases with the cutting speed in both CM and MAM turning. At V_c = 150 m/min, the tool temperature is slightly higher in MAM than in CM turning. However, at higher speeds, the tool temperature is significantly lower in MAM than in CM turning. Therefore, the reduction in temperature by MAM turning is more effective at the higher cutting speeds. This matches well with the wear results that wear reduction by MAM turning is more significant at the higher cutting speeds.

Figure 12a shows the tool temperature history in all cutting intervals for CM and MAM turning at V_c = 350 m/min. In general, all these temperature curves show the same trend, i.e., an initial rapid increase in temperature smoothly transitioned to a steady state increase in temperature with a lower rate. The changes in the temperature from one interval to another should reflect the tool wear effect on the cutting temperature. In CM turning, the temperature curve for the 2nd interval is significantly higher than the curve for the 1st interval, which is due to the rapid tool wear and severe adhesion occurring during the 2nd interval. In MAM turning, the temperature curve is elevated in general from one interval to another. However, the temperature curve even for the 6th interval in MAM turning is still not higher than the temperature curve for the 1st interval in CM turning. This slow temperature elevation with cutting interval can be attributed to the mild wear progression in MAM turning.

More careful observation reveals that the temperature elevation from one interval to another is not uniform in MAM turning. The temperature curve for the 2nd interval has a significantly lower ramp in the steady state region which leads to a temperature reduction compared to the 1st interval. The temperature curve for the 3rd interval is elevated higher than the

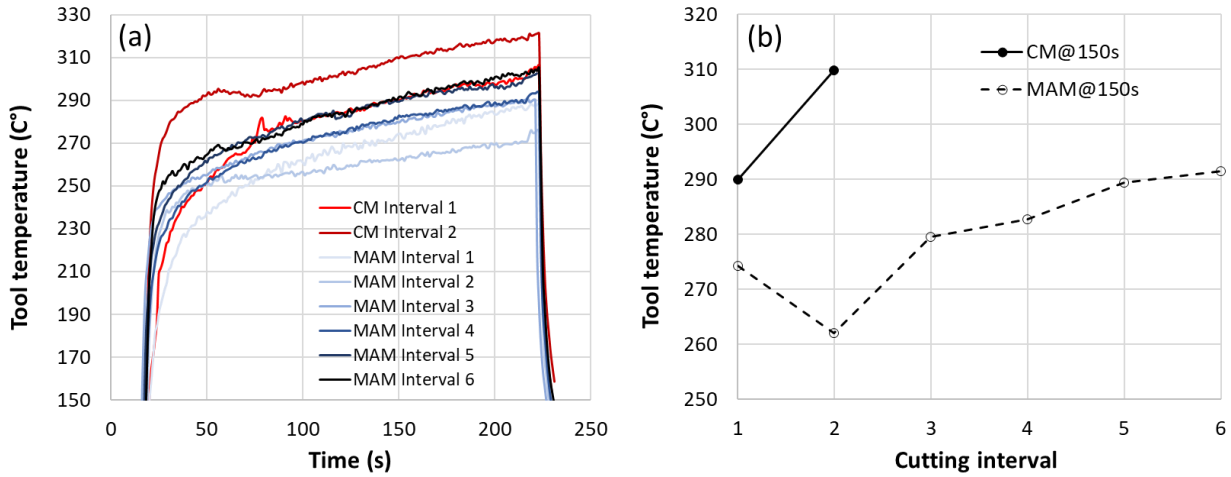

Fig. 12. (a) Tool temperature history during each cutting interval in CM (red) and MAM (blue) turning at V_c = 350 m/min. The color gets darker with increasing interval. (b) The temperature value at t = 150s in each temperature history curve in (a).

curve for the 1st interval. The temperature curve for the 4th interval is not significantly elevated from the 3rd interval. The temperature curve for the 5th interval is elevated again while the temperature curve for the 6th is not significantly elevated from the 5th interval. Both curves from the 5th and the 6th intervals nearly overlap with the curve for the 1st interval in CM turning in the steady state region. To better show the temperature elevation from one interval to another, the temperature value at time = 150 s for each curve in Fig. 12a (which is in the steady state region) is used as a representative temperature for the corresponding cutting interval. Figure 12b plots this representative temperature versus the cutting interval. It is evident that MAM turning results in lower tool temperature, and the increase in tool temperature with cutting interval is also more gradual in MAM than in CM turning. These results match generally well with the wear progression in CM and MAM turning, indicating again the close correlation between the temperature and the wear.

5. Summary

In this study, a new MAM turning setup has been implemented to conduct longitudinal turning experiments on CGI with coated carbide tools. Tool wear, cutting forces and temperature are experimentally characterized in CM and MAM turning at three cutting speeds (150, 250 and 350 m/min). The findings of this study can be summarized as follows:

The primary wear in cutting CGI with coated carbide tool is the flank wear in both CM and MAM turning. The flank wear is not reduced by MAM at the low cutting speed (150 m/min). However, at the higher cutting speeds (250 and 350 m/min), the flank wear is significantly lower in MAM than in CM turning, and the reduction in tool wear by MAM is even more significant when measured by wear volume.

Severe iron adhesion occurs when the tool coating is breached, which leads to the rapid wear in CM turning at the higher speeds (250 and 350 m/min). In CM turning, the breach of tool coating accompanied by severe iron adhesion tends to start in the middle region of the side cutting edge and very rapidly spread toward the nose region and the end region of side cutting edge.

The breach of coating with iron adhesion also occurs in MAM turning. However, it tends to start separately on the tool nose region and the end region of the side cutting edge, and then spread gradually toward the middle region of the side cutting edge. Increasing the cutting speed will accelerate this wear process, but the speed effect is far less significant in MAM than in CM turning. As a result, the reduction in wear by MAM is most effective at the higher cutting speeds.

The increase in the flank wear leads to the increase in both the primary cutting force and the feed force. However, the wear effect is much more significant on the feed force than the primary cutting force, which is consistent with the fact that the dominant wear is the flank wear. Besides the size of the flank wear land, the severity of the adhesion also contributes to the wear effect on the forces.

Tool temperature is significantly lower in MAM than in CM turning at the higher cutting speeds, but slightly higher at the low cutting speed, which agrees with the wear comparison in MAM and CM turning at the low and higher speeds. This indicates the reduction in tool temperature is an important reason for the reduction in tool wear in MAM turning.

Acknowledgements

This work is supported by NSF CMMI grant no. 2019320. We thank Ryan Khawarizmi for helping with the etching of the tools.

References

[1] Dawson SinterCast S. Compacted Graphite Iron-A Material Solution for Modern Diesel Engine Cylinder Blocks and Heads. 68th WFC-World Foundry Congr., 2008, p. 93–9.

[2] Dawson S. Compacted graphite iron: mechanical and physical properties for engine design. VDI Berichte 1999;1472:85–106.

[3] Dawson S, Hollinger I, Robbins M, Daeth J, Reuter U, Schulz H. The effect of metallurgical variables on the machinability of compacted graphite iron. SAE Tech. Pap., 2001. https://doi.org/10.4271/2001-01-0409.

[4] Abele E, Sahm A, Schulz H. Wear mechanism when machining compacted graphite iron. CIRP Ann - Manuf Technol 2002;51.

https://doi.org/10.1016/S0007-8506(07)61464-4.

[5] Nayyar V, Grenmyr G, Kaminski J, Nyborg L. Machinability of compacted graphite iron (CGI) and flake graphite iron (FGI) with coated carbide. Int J Mach Mach Mater 2013;13:67–90. https://doi.org/10.1504/IJMMM.2013.051909.

[6] Phillips CW. Machinability of compacted graphite iron.(Retroactive Coverage). Trans Am Foundrymen's Soc 1982;90:47–52.

[7] Gastel M, Konetschny C, Reuter U, Fasel C, Schulz H, Riedel R, et al. Investigation of the wear mechanism of cubic boron nitride tools used for the machining of compacted graphite iron and grey cast iron. Int J Refract Met Hard Mater 2000;18:287–96.

[8] Stephenson DA, Agapiou JS. Metal cutting theory and practice. CRC press; 2016.

[9] Stephenson DA, Ali A. Tool temperatures in interrupted metal cutting. J Manuf Sci Eng Trans ASME 1992;114:127–36. https://doi.org/10.1115/1.2899765.

[10] Tooptong S, Park K-H, Kwon P. A comparative investigation on flank wear when turning three cast irons. Tribol Int 2018;120:127–39. https://doi.org/10.1016/j.triboint.2017.12.025.

[11] Heck M, Ortner HM, Flege S, Reuter U, Ensinger W. Analytical investigations concerning the wear behaviour of cutting tools used for the machining of compacted graphite iron and grey cast iron. Int J Refract Met Hard Mater 2008;26. https://doi.org/10.1016/j.ijrmhm.2007.05.003.

[12] de Sousa JAG, Sales WF, Machado AR. A review on the machining of cast irons. Int J Adv Manuf Technol 2018;94. https://doi.org/10.1007/s00170-017-1140-1.

[13] Abdoos M, Rawal S, Arif AFM, Veldhuis SC. A strategy to improve tool life by controlling cohesive failure in thick TiAlN coating during turning of CGI. Int J Adv Manuf Technol 2020;106. https://doi.org/10.1007/s00170-019-04854-0.

[14] de Oliveira V V., Beltrão PA d. C, Pintaude G. Effect of tool geometry on the wear of cemented carbide coated with TiAlN during drilling of compacted graphite iron. Wear 2011;271. https://doi.org/10.1016/j.wear.2010.12.075.

[15] Mann JB, Guo Y, Saldana C, Compton WD, Chandrasekar S. Enhancing material removal processes using modulation-assisted machining. Tribol Int 2011;44:1225–35.

[16] Guo Y, Mann JB, Yeung H, Chandrasekar S. Enhancing Tool Life in High-Speed Machining of Compacted Graphite Iron (CGI) Using Controlled Modulation. Tribol Lett 2012;47:103–11. https://doi.org/10.1007/s11249-012-9966-z.

[17] Guo Y, Stalbaum T, Mann J, Yeung H, Chandrasekar S. Modulation-assisted high speed machining of compacted graphite iron (CGI). J Manuf Process 2013;15. https://doi.org/10.1016/j.jmapro.2013.06.001.

[18] Sahm A, Abele E, Schulz H. Machining of compacted graphite iron (CGI). Materwiss Werksttech 2002;33:501–6. https://doi.org/10.1002/1521-4052(200209)33:9<501::AID-MAWE501>3.0.CO;2-W.

[19] Deyuan Z, Lijiang W. Investigation of chip in vibration drilling. Int J Mach Tools Manuf 1998. https://doi.org/10.1016/s0890-6955(97)00047-3.

[20] Guo Y, Mann JB. Control of Chip Formation and Improved Chip Ejection in Drilling With Modulation-Assisted Machining. J Manuf Sci Eng 2020;142. https://doi.org/10.1115/1.4046829.

[21] Moscoso W, Olgun E, Compton WD, Chandrasekar S. Effect of Low-Frequency Modulation on Lubrication of Chip-Tool Interface in Machining. J Tribol 2005;127:238–44. https://doi.org/10.1115/1.1829720.

[22] Yeung H, Guo Y, Mann JB, Compton WD, Chandrasekar S. Effect of low-frequency modulation on deformation and material flow in cutting of metals. J Tribol 2016;138:12201.

[23] Park KH, Kwon PY. Flank wear of multi-layer coated tool. Wear 2011;270:771–80. https://doi.org/10.1016/j.wear.2011.01.030.

[24] Olortegui-Yume JA, Kwon P. Crater wear evolution in multilayer coated carbides during machining using confocal microscopy. J Manuf Process 2007;9:47–60. https://doi.org/10.1016/S1526-6125(07)70107-X.